



1 Characterization of three new condensation particle counters for sub-3 nm particle detection: ADI
2 versatile water CPC, TSI 3777 nano enhancer and boosted TSI 3010

3

4 Juha Kangasluoma¹, Susanne Hering², David Picard³, Greg Lewis², Joonas Enroth¹, Frans Korhonen¹,
5 Markku Kulmala¹, Karine Sellegri³, Michel Attoui^{1,4}, Tuukka Petäjä¹

6

7 ¹ Department of Physics, P.O. Box 64, 00014, University of Helsinki, Helsinki, Finland

8 ² Aerosol Dynamics Inc., Berkeley, CA, USA

9 ³ Laboratoire de Météorologie Physique, UMR6016, Observatoire de Physique du Globe de
10 Clermont-Ferrand, CNRS – Université Blaise Pascal, Clermont-Ferrand, France

11 ⁴ University Paris Est Creteil, University Paris-Diderot, LISA, UMR CNRS 7583, France

12

13 Abstract

14

15 The scientific need to understand nanoparticle dynamics at sizes below 3 nm has pushed companies
16 to develop commercial solutions to measure particles down to 1 nm. In this study we characterize the
17 performance of three new particle counters able to detect particles smaller than 3 nm: Aerosol
18 Dynamics Inc versatile water condensation particle counter (v-WCPC, ADI, Berkeley, USA), TSI 3777
19 nano enhancer (TSI Inc., Shoreview, USA) and modified and boosted 3010 type CPC from Clermont
20 Ferrand University called as B3010. The 3777 and v-WCPC were characterized using tungsten oxide
21 test particles with all charging states: negative, positive and neutral, and with positively charged
22 tetradodecylammonium bromide. The detection efficiencies of the particle counters were measured
23 with two different temperature settings: low temperature difference settings so that the CPCs did not
24 detect any ions from a radioactive source; and high temperature difference settings so that the
25 supersaturation was at the onset of homogeneous nucleation for the 3777, or confined within the
26 range of liquid water for the ADI v-WCPC. The measured 50% detection diameters (d_{50}) were in the
27 range of 1.3 – 2.4 nm for the tungsten oxide particles depending on the particle charging state and
28 CPC temperature settings, and between 2.5 and 3.3 nm for the organic test aerosol for the 3777 and
29 v-WCPC. The d_{50} s were measured for the B3010 with negatively charged tungsten oxide particles with
30 four different inlet flow rates. The v-WCPC and 3777 were also compared side by side by measuring
31 atmospheric aerosol, exhibiting an excellent agreement.

32

33 1 Introduction

34

35 The work of Stolzenburg and McMurry (1991) started a new chapter in aerosol research with their
36 prototype laminar flow condensation particle counter (CPC) capable of detecting 3 nm particles via
37 condensation of butanol vapor. The significant improvements in the instrument included minimized
38 diffusion losses in the sampling line and a sheath flow in the condenser to focus the particle beam in
39 the maximum butanol supersaturation in the middle of the condenser (Wilson et al., 1983). This
40 instrument is the predecessor of the ultrafine CPC 3025A and 3776 (TSI Inc., Shoreview, USA), which
41 currently are widely used in various fields of aerosol science to study particle dynamics at particle sizes
42 larger than 3 nm (e.g. Aalto et al., 2001; Weber et al., 1996).

43

44 It was not possible to detect particles smaller than 3 nm with the CPC technology until 1997,
45 when Seto et al. (1997) published their design on the particle size magnifier (PSM) used to study
46 heterogeneous nucleation of dibutyl phthalate vapor onto small ions. Their advances were made
47 possible by the development of a new differential mobility analyzer (DMA) combined to an
48 electrospray source, allowing the testing of the CPC with well-characterized monomobile samples. The
49 CPC itself was based on the design of Okuyama et al. (1984), which is a mixing type CPC. It took until
50 2011 to commercialize the mixing type CPC technology, when Vanhanen et al. (2011) published their
51 version of the diethylene glycol (DEG) based PSM, today sold as the Airmodus A10 PSM (A11 nano
condensation nuclei counter when combined to Airmodus A20 butanol CPC).



52 The first use of DEG as a working fluid was by Iida et al. (2009), who studied sub-3 nm particle
53 detection with various different working fluids theoretically and experimentally. They modified the
54 TSI 3025A to operate with DEG and showed particle activation and growth down to 1 nm. Because the
55 DEG droplets formed are small, a traditional, butanol based CPC is used as a detector. The idea of
56 using the commercial TSI instrument with modifications to operate with DEG has been followed by
57 several other researchers (Jiang et al., 2011a; Jiang et al., 2011b; Kuang et al., 2012a; Kuang et al.,
58 2012b; Wimmer et al., 2013). In 2016 TSI commercialized a DEG instrument based on the work of Iida
59 et al. (2009). This instrument, the TSI 3777 nano enhancer (3777), is one of the three instruments
60 characterized in this study.

61 Generally, laminar flow ultrafine CPCs use a sheathed condenser, which makes the CPC design
62 more complex compared to non-sheathed CPCs. Yet recent efforts have shown lower detection limits
63 with unsheathed laminar-flow instruments. Particle detection with the butanol-based TSI 3010 has
64 been shown down to 2.5 nm from the factory settings d_{50} (diameter at which 50% of sampled particles
65 are detected) of 10 nm (Mertes et al., 1995; Russell et al., 1996; Wiedensohler et al., 1997).
66 Kangasluoma et al. (2015a) showed 1 nm particle detection with the commercial unsheathed
67 condenser CPCs TSI 3772 and Airmodus A20 by increasing the temperature difference between the
68 saturator and condenser up to 40 °C. The second CPC characterized in this study is a boosted TSI 3010
69 (B3010), which is a modification of the commercial TSI3010 developed at the Université Blaise Pascal
70 in which the temperature control of the saturator and condenser is decoupled to allow free selection
71 of the temperatures, and critical orifice is replaced with a flow meter and a miniature rotary vane
72 pump.

73 The disadvantage of all the previous CPCs is the slight toxicity of the working fluids butanol
74 and DEG. Hering et al. (2005) addressed this issue by developing a water based, laminar technology
75 (Hering and Stolzenburg, 2005), which was commercialized as the TSI WCPC models 3785 (Hering et
76 al., 2005) and 3786 (Iida et al, 2008), and subsequently as the 3783, 3787 and 3788. In the Model 3786,
77 and later in the Model 3788 (Kupc et al., 2013), small particle detection was enabled by introducing
78 similar sheathed condenser as in the butanol based CPCs

79 The ADI versatile WCPC (v-WCPC), which is the third CPC characterized in this study, advances
80 the laminar-flow water-based CPC through a three stage design that reduces the water vapor
81 concentration and temperature in the growth tube after the peak supersaturation is achieved, and
82 yet allows for continued particle growth (Hering et al., 2016). This three-stage approach facilitates
83 higher temperature differences between the first two stages, and can produce higher peak
84 supersaturation values than the ultrafine TSI 3786 or TSI 3788. The v-WCPC is an unsheathed
85 instrument, operating at an aerosol flow of 0.3 litres per minute (lpm) and at more extreme
86 temperatures than all of the current commercial TSI WCPCs. In contrast to the DEG-based instruments,
87 which require a separate CPC as a detector due to the small size of the DEG droplets, the droplets
88 formed in the growth tube of the v-WCPC are sufficiently large to be detected directly.

89 The aim of this study is to characterize the performance of the v-WCPC and 3777 with two
90 different types of test particles, to measure effect of charge to the detection efficiency and to compare
91 the instrument responses in atmospheric sampling. The performance of the B3010 was characterized
92 with tungsten oxide particles for different aerosol flow rates.

94 2 Experimental

96 2.1 Condensation Particle Counters

97
98 A flow diagram of the 3777 is presented in Figure 1. The design is largely similar to the TSI ultrafine
99 3776. The inlet flow rate is 2.5 lpm, of that 1.5 lpm being transport flow and 1 lpm split as the sheath
100 flow (0.85 lpm) and aerosol flow (0.15 lpm). The sheath flow passes through a dessicant drier to
101 remove most water vapor entering the condenser, possibly altering the detection efficiency of a DEG
102 based CPC (Iida et al., 2009; Kangasluoma et al., 2013). Downstream of the drier the sheath flow is



103 saturated with DEG before entering the condenser around the aerosol flow, which is guided in the
104 centre line of the condenser. The 3777 does not have its own optics head, as the droplets formed by
105 DEG condensation are too small for direct detection. Instead the detector is a TSI 3772 CPC, which
106 further enlarges and then counts the droplets pre-grown by DEG in the condenser. The factory settings
107 of the 3777 are: saturator 62 °C and condenser 12 °C (low temperature difference (dT) settings). At
108 these settings the 3777 did not detect any ions produced by a radioactive ²⁴¹Am source. It was also
109 operated at boosted settings so that the supersaturation was at the onset of homogeneous
110 nucleation. With the boosted settings the saturator was 70 °C and condenser 7 °C (high dT settings).

111 Flow diagram of the ADI v-WCPC is presented in Figure 2. The v-WCPC does not require a
112 separate CPC for droplet detection, nor does it use a sheath flow, making it a relatively simple CPC.
113 The v-WCPC has two flows, a transport flow and an aerosol flow, both of which are controlled by
114 critical orifices. For experiments conducted here the inlet flow rate of the v-WCPC was 2.2 lpm, of
115 which 1.9 lpm is transport flow and 0.3 lpm aerosol flow. The aerosol flow passes upward through a
116 three-stage growth tube consisting of a cool-walled conditioner, followed by a short, warm-walled
117 initiator, and subsequently followed by a cool-walled moderator (Hering et al., 2014). A continuous
118 wick spans all three growth tube sections. Liquid water is injected at a rate of 1 µL/min at the initiator,
119 and excess drains toward the inlet and is removed with the transport flow. Peak supersaturation and
120 particle activation occurs within the initiator, and growth continues in the moderator. The formed
121 droplets are counted by an optics head mounted directly at the outlet of the growth tube. Further
122 detail is presented by Hering et al. (2016). The v-WCPC was tested at two different temperature
123 settings: conditioner at 8 °C and initiator at 90 °C (low dT settings), corresponding to supersaturation
124 low enough to not detect any ions from a radioactive source, and boosted settings with conditioner
125 at 1 °C and initiator at 95 °C (high dT settings), which is close to the extremes attainable without
126 freezing or boiling. In both instances the moderator was operated at 22°C, and the optics head at 40°C.

127 The B3010 is based on a cheap second hand TSI 3010, from which everything except the
128 saturator block, the condenser and the optical detector are removed. The original electronics have
129 been completely replaced with custom made boards, to handle the higher power consumption, and
130 operate off 28 VDC, the primary power supply in aircrafts. The whole system is controlled by a credit
131 card sized ARM computer, running a tailor-made embedded Linux operating system. It features a
132 touchscreen, a TSI-like serial port protocol, and TTL pulse output. With these modifications the
133 saturator heating and condenser cooling are decoupled. In addition, the critical orifice and external
134 heavy pump are replaced by a laminar flowmeter and a miniature rotary vane pump. The user may set
135 the temperature of the saturator, condenser and optics as well as the flow rate, independently from
136 one another. The B3010 was operated at saturator temperature 55 °C, optics head 56 °C and condenser
137 11 °C. The B3010 will be described in more details in a dedicated article, presently in preparation. Table
138 1 summarizes the instrument operation conditions.

139

140 2.2 Aerosol generation

141

142 Two methods were used to generate the test aerosol: glowing wire generator (GWG) and electrospray
143 source. In the GWG (Peineke et al., 2006), a thin, 0.4 mm in diameter, tungsten wire is heated
144 resistively in a metal chamber. The wire is flushed with 5.0 N₂ flow and it has been shown that
145 negatively charged tungsten oxide clusters are formed into the N₂ flow without additional charging
146 (Kangasluoma et al., 2015b). Positively charged clusters contain some hydrocarbon molecules
147 clustered with tungsten oxide, explaining why usually the measured d₅₀ usually is larger for positively
148 than negatively charged clusters (Kangasluoma et al., 2016b). The d₅₀ for all three CPCs, at two
149 different temperature settings for the 3777 and v-WCPC and at one settings for the B3010, was
150 measured with tungsten oxide particles by size selecting 18 different sizes of particles between 1 and
151 4.5 nm with the Herrmann type high resolution DMA (Kangasluoma et al., 2016a) (Figure 4). The tubing
152 lengths downstream of the DMA were selected to be equal for the vWCPC, 3777 and electrometer so
153 that the particle penetration through the tubes can be considered equal. For the B3010 the line length



154 was approximately half of the electrometer tubing for the same reason. The d50 of the 3777 was
155 measured at four different sample flow dew points with negatively charged tungsten oxide particles.
156 Water vapor was added to the sample flow with a humidified dilution flow downstream of the DMA.
157 The d50 for the B3010 was measured also at four different aerosol flow rates, 0.5, 1.0, 1.4 and 1.6
158 lpm, by varying the rotary vane pump speed.

159 The electro spray source produces charged sample molecule containing droplets by spraying
160 liquid at high voltage out of a capillary needle against a grounded electrode. The charged droplets are
161 close to the Rayleigh limit, and produce charged sample molecules and clusters to the gas flow by
162 series of Coulomb explosions, and ion and solvent evaporation from the droplet. The highly charged
163 droplets can be close to 2 nm in mobility diameter (Ude and Fernández de la Mora, 2005), for which
164 we neutralized the flow exiting the electro spray with a radioactive ^{241}Am source to also be able to
165 sample the clusters larger than 2 nm (Kangasluoma et al., 2016a). The electro sprayed sample in the
166 experiments was tetradodecylammonium bromide (TDDABr) (Ude and Fernández de la Mora, 2005).
167 d50 was measured for the 3777 and v-WCPC with TDDABr with the low dT settings, and for the v-
168 WCPC at the high dT settings. For the 3777 we could not measure the d50 at high dT settings due to
169 the fact that the aerosol-to-sheath flow ratio is very sensitive to the CPC inlet pressure, and TDDABr
170 was produced by drawing the flow out of the DMA, leading to a pressure drop of approximately 5 kPa
171 at the CPC inlets. This pressure drop was enough to alter the aerosol-to-sheath flow ratio in the 3777
172 and cause homogeneous droplet formation at high dT settings.

173 To measure the d50 for neutral particles, we followed the approach presented in our previous
174 studies (Kangasluoma et al., 2015b; Kangasluoma et al., 2016b). The sample flow downstream of the
175 DMA passes through a mixing chamber, to which a tube containing a ^{241}Am radioactive is connected.
176 0.2 lpm of the sample flow is drawn through the tube, and ions from the radioactive source are drifted
177 to the mixing chamber against the counter flow with an electric field. A fraction of the sample particles
178 are neutralized by the opposite polarity ions drifted to the mixing chamber. An ion precipitator is
179 placed downstream of the mixing chamber to allow sampling of only neutral particles with the CPC.
180 The concentration detected with the CPC is normalized against the electrometer. The detection
181 efficiency curve is further normalized with detection efficiency of the largest selected diameters where
182 the role of charge on the detection efficiency is assumed to be negligible. This method yields
183 uncertainties in the resulting d50 due to possibly size dependent neutralization efficiency and
184 chemical composition of the neutralized particles, however, it is being the only method to measure
185 d50 for neutral particles for sub-3 nm particles. Neutral d50 was measured for both instruments with
186 high and low dT by neutralizing both negatively and positively charged particles.

187

188 2.3 Ambient sampling setups

189

190 The response of the v-WCPC was measured against the TSI electrometer (model 3068B) at different
191 concentrations at sizes 1.4nm, 1.8nm, 2.4nm and 4.4 nm. The concentration at each size was
192 controlled by adding a dilution flow of compressed and filtered air downstream of the DMA.
193 Simultaneous data were collected for the 3777, however the dilution flow was enough to change the
194 aerosol-to-sheath flow ratio of the 3777 due to a small change in the inlet pressure, and therefore the
195 3777 data of this experiment are not presented. However, assuming that any possible undercounting
196 at high concentration originates from particle coincidence in the optics, the concentration calibration
197 of the 3777 should be practically the same as of the 3772 CPC when the dilution of 0.15/1 is taken into
198 account.

199 Finally, the 3777 and v-WCPC were placed to sample atmospheric aerosol from Helsinki city
200 area. The instruments were sampling from the same inlet for approximately 18 h to compare the
201 measured concentrations from atmospheric aerosol. The v-WCPC data were dead-time corrected
202 using the dead time correction factor derived from the concentration dependent response for 4.4 nm.

203

204 3 Results



205

206 3.1 Detection efficiency

207

208 Figure 5 presents the d_{50} measurements for the B3010, 3777 and v-WCPC at low dT settings for
209 positively and negatively charged tungsten oxide particles. The standard deviation in the detection
210 efficiency data was in most cases $< 5\%$, which is why it is not plotted in the figures. X-axis uncertainty
211 can be taken from the Herrmann DMA resolution of approximately 20, which leads to relative
212 uncertainty of $\pm 5\%$ based on the selected mobility peak full width at half maximum of 5%. Therefore,
213 uncertainties in the data arise mostly from other sources, such as unequal sampling line penetration
214 or possibly changing particle chemical composition as a function of size. At these settings none of the
215 CPCs detect the ions generated by a bipolar ion source, such as is commonly used for mobility based
216 particle size distribution measurements. We find that the v-WCPC exhibits slightly lower d_{50} than the
217 3777, while the d_{50} of the B3010 is clearly the highest. The d_{50} of 3.2 – 3.4 nm for the B3010 however
218 shows that the conventional TSI 3010 can be boosted to similar performance as the TSI ultrafine 3776,
219 just with a shallower d_{50} curve due to larger particle diffusion losses, by decoupling the heating and
220 cooling of the saturator and condenser. Respective d_{50} values for the B3010, v-WCPC and TSI-3777
221 are 3.4 nm, 1.7 nm and 1.8 nm for negatively charged tungsten oxide, and 3.2 nm, 1.9 nm and 2.0 nm
222 for positively charged.

223

224 At high dT settings the d_{50} curves are presented in Figure 6. For the 3777 the temperatures
225 were selected as those that are just below the limit of homogeneous nucleation of the DEG working
226 fluid. For the v-WCPC, the temperatures are simply the largest extremes attainable without freezing
227 or boiling the water working fluid. Unlike the DEG instrument, the high dT operation of the v-WCPC
228 is not near the homogeneous nucleation limit, as no evidence of homogeneous nucleation was
229 observed even at reduced inlet pressures. At these higher dT settings, we find somewhat more
230 efficient detection of smaller particles by the 3777 than the v-WCPC. The d_{50} s are lowered to 1.4 nm
231 and 1.3 nm for negatively charged, and to 1.5 nm and 1.4 nm for positively charged for the v-WCPC
232 and 3777, respectively.

233

234 Table 2 summarizes the measured d_{50} for all experiments. The d_{50} for 3777 and v-WCPC at
235 both settings is lower for negatively charged particles than for positively charged particles. This is
236 observed throughout the past literature (Kangasluoma et al., 2014; Kuang et al., 2012b; Sipilä et al.,
237 2009; Stolzenburg and McMurry, 1991; Winkler et al., 2008), and explained by hydrocarbon
238 contaminants in the positively charged particles (Kangasluoma et al., 2016b). Based on previous
239 literature (Kangasluoma et al., 2014; Kuang et al., 2012b) slightly lower d_{50} values can be expected
240 for inorganic salt particles than the measured d_{50} s for tungsten oxide particles in this study. TSI states
241 in their instrument brochure a d_{50} of 1.4 nm for negatively charged NaCl particles at factory settings
242 (low dT in this study), which is well in line with this study. Similarly, the d_{50} values reported here for
243 the v-WCPC are close to those observed by Hering et al. (2016) who measured d_{50} of 1.6 nm and
244 1.9 nm for high dT and low dT operation, respectively, for particles from a heated NiCr wire.

245

246 Figure 7 presents the d_{50} curves for the neutralized tungsten oxide particles. The data is
247 normalized so that the mean of 3 largest diameters is 90% based on the assumption that at those sizes
248 the charge does not affect the detection efficiency anymore. Also is assumed, through the
249 normalization that the neutralization efficiency does not change as a function of the particle size.
250 Further uncertainties arise from the unknown processes that take place during neutralization. Due to
251 these uncertainties, the curves are not as smooth as for the charged particles. However, an estimate
252 for the neutral d_{50} will be obtained from these experiments, which are 1.6 nm and 1.5 nm for v-WCPC
253 and 3777 at high dT , and 2.0 nm and 1.9 nm at low dT settings, respectively, for neutralized negatively
254 charged tungsten oxide. For positively charged particles the respective values are 2.2 nm and 2.1 nm
255 at high dT settings and 2.4 nm and 2.3 nm at low dT settings (Figure 9). The neutral d_{50} s are greater
256 than for charged d_{50} values by approximately 0.1-0.5 nm at low dT settings, similar to that obtained
257 in Kangasluoma et al. (2016b) for water-tungsten oxide and DEG-tungsten oxide system.



255 The d50 curves for positively charged TDDABr for the 3777 and v-WCPC are presented in
256 Figure 9. For both instruments the d50 values are higher than for tungsten oxide particles, but this is
257 most pronounced for the v-WCPC. At the low dT settings d50 values are 3.3 nm and 2.5 nm at for the
258 v-WCPC and 3777 respectively, and 2.8 nm for the v-WCPC at high dT. At the high dT and the reduced
259 inlet pressure for these TDDABr tests, the 3777 produced homogeneously nucleated particles, and
260 hence its high dT d50 value could not be measured. These differences in the d50 imply that the CPCs
261 should be calibrated with the same aerosol composition as with the real experiment is conducted.

262

263 3.2 Effect of sample dew point for the 3777

264

265 Because water-contamination was observed as a source of error in the original laminar-flow DEG
266 instruments, this question was examined for the 3777. The response of the 3777 for negatively
267 charged tungsten oxide particles as a function of sample flow dew point is presented in Figure 10. The
268 observed variation with dew points ranging from completely dry gas to 20 °C in the d50 is only
269 approximately 0.1 nm. The apparently increased plateau value for the highest dew point can be due
270 to slightly higher inlet pressure, increasing the aerosol flow of the instrument. The variation in the d50
271 due to changing dew point is less than compared to for example 0.3 nm reported in Kangasluoma et
272 al. (2013) for the Airmodus A09 PSM. This is due to the smaller amount of sample flow water vapor
273 reaching the condenser in the 3777, since 85% of the condenser flow is dried, as compared to 0% of
274 the condenser flow of the PSM of that time. At that time the PSM used internal pumps, today they are
275 replaced by mass flow controllers which are usually fed by dry compressed air, resulting to dried
276 condenser flow fraction from 4% to 34% depending on the instrument operation.

277

278 3.3 Effect of flow rate on the B3010

279

280 Results from the inlet flow rate experiment for the B3010 is presented in Figure 11. The d50 curve at
281 aerosol flow rates of 0.5, 1, 1.4 and 1.6 lpm are rather similar within the experimental uncertainties,
282 while at flow rate of 0.5 the detection efficiency clearly deviates to lower values at particle diameters
283 larger than 3 nm. This can be possibly due to larger final droplet diameters and subsequent
284 gravitational losses at the low flow rate. Similar increase in the detection efficiency with higher flow
285 rate as in Kangasluoma et al. (2015a) was not observed, which can be due to the differences in the
286 saturators between the 3010 and 3772: 3010 has a single hole reservoir type saturator while 3772 has
287 8 hole multitube saturator which possibly saturates the sample flow better than the one hole saturator
288 at higher flow rates.

289

290 3.4 Concentration calibration

291

292 As with all CPCs, the peak supersaturation, and hence the lowest detectable particle size is can be
293 affected by the presence of other particles in the flow, due to a combination of condensational heat
294 release and vapor depletion. These effects for the original WCPCs were explored by Lewis and Hering
295 (2013), and is evaluated here for the v-WCPC. Figure 12 shows the concentration dependent response
296 at four particle sizes for the v-WCPC. The maximum concentration at each size was determined by the
297 maximum concentration we were able to pass through the DMA. The data are corrected for dead
298 time, as described by Hering et al. (2005), and as is standard for most of the commercial CPCs. This
299 approach uses the instrument dead time multiplied by a dead time correction factor, which accounts
300 for the increase in effective dead time due to overlapping tails in pulses below the threshold. For this
301 data set the dead time correction factor was set to 1.23 to yield a linear response to concentration at
302 4.4 nm. Then this same dead time correction factor was applied to measurements at other sizes. The
303 curves of the three smallest particle sizes have a negative slope due to the reduction in
304 supersaturation at high concentrations caused by condensational heating (Lewis and Hering, 2013).



305 However, the effect is relatively small, with the detection at 1.8 nm dropping from 36% at a
306 concentration of 3000cm^{-3} to 33% at a concentration of 90000cm^{-3} .

307

308 3.5 Atmospheric sampling

309

310 A fraction of the data measured from atmospheric aerosol is presented in Figure 13. The measurement
311 location is above a bus stop, which several busses pass daily through. The bus stop times are marked
312 to the figure. The background aerosol concentration during that morning was around $3\,000 - 10\,000$
313 cm^{-3} . Clear spikes up to $200\,000\text{cm}^{-3}$ in the measured concentrations are observed throughout the
314 morning, of which timing match quite well the scheduled bus departure times. From the data of Figure
315 13, a correlation plot between the v-WCPC and 3777 is presented in Figure 14 for concentrations
316 below $50\,000\text{cm}^{-3}$. With R^2 of 0.99 the two CPCs show remarkably good agreement with slope of 1.02
317 and offset of 340 up to concentrations of $50\,000\text{cm}^{-3}$.

318

319 4 Conclusions

320

321 Three new sub 3 nm CPCs, boosted 3010 type CPC, ADI versatile water CPC and the TSI 3777 nano
322 enhancer were characterized for the d_{50} diameter. The boosted 3010 type CPC was shown to be able
323 to detect tungsten oxide particles smaller than 3 nm. The vWCPC and 3777 were characterized with
324 similar test aerosols with two different settings: low dT settings set so that the CPCs did not detect
325 any ions from a radioactive charger, and high dT settings set either so that the supersaturation was at
326 the onset of homogeneous droplet formation (3777) or set to the largest value that avoids freezing or
327 boiling (v-WCPC). The d_{50} diameters for tungsten oxide were found to range from 1.7 nm to 2.4 nm
328 at low dT and from 1.4 nm to 2.2 nm at high dT for the v-WCPC. For the 3777 the d_{50} ranged from 1.8
329 nm to 2.3 nm at low dT and from 1.3 nm to 2.1 nm at high dT. Both CPCs were observed to detect
330 charged tungsten oxide particles better than neutral ones. The organic salt particles (TDDABr) were
331 detected less efficiently, with low dT d_{50} diameters of 3.3 nm for the v-WCPC, and 2.5 nm for the TSI-
332 3777. When measuring the same atmospheric aerosol the two CPCs showed a very good agreement
333 with regression slope of 1.02 and R^2 of 0.99.

334 From the results we can make the following conclusions: The TSI 3010 hardware can be tuned
335 to accomplish 3 nm particle detection by increasing the dT but not by increasing the inlet flow rate,
336 which is in line with Buzorius (2001). This is possibly due to not perfect flow saturation in the reservoir
337 type saturator as opposed to the multihole saturator of TSI 3772 and planar type saturator of
338 Airmodus A20 (Kangasluoma et al., 2015a). Due to the variations in the d_{50} with composition for the
339 vWCPC and 3777, their use as a detector downstream of a DMA is suggested only if the particle
340 composition is known and CPC calibration is made accordingly with the same particle composition, or
341 with sizes above the highest d_{50} (approximately 2.5 – 3 nm) if the particle composition is completely
342 unknown. The effect of particle charge on the d_{50} was show to be up to approximately 0.5 nm, which
343 has implications on to system characterizations where the fraction of charged particles can be
344 expected to be high (Wang et al., 2017), or CPC calibration is conducted with charged particles and
345 sampled particles are neutral, and high precision d_{50} is required.

346

347 Acknowledgements

348

349 The authors acknowledge TSI Inc. who provided the control boards and optics for the v-WCPC, and
350 who loaned the TSI 3777 for these experiments. The research was partly funded by European Research
351 Council (ATMNUCLE, 227463), Academy of Finland (Center of Excellence Program projects 1118615
352 and 139656), European Commission seventh Framework program (ACTRIS2 contract no 654109, PPP
353 and EUROCHAMP-2020), Labex ClerVolc contribution n° 228 and Maj and Tor Nessling Foundation.

354

355 References



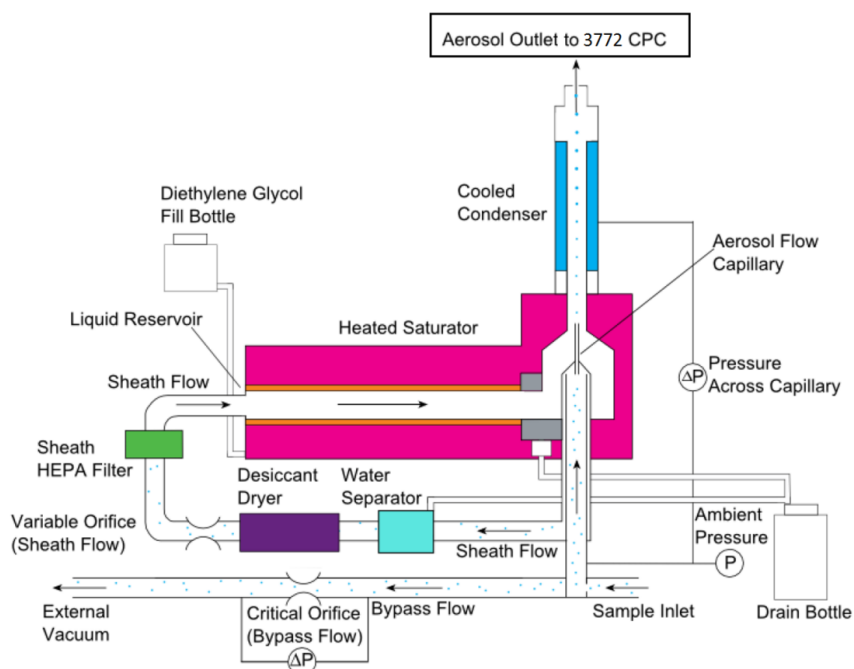
- 356
357 Aalto, P., Hameri, K., Becker, E., Weber, R., Salm, J., Makela, J. M., Hoell, C., O'Dowd, C. D., Karlsson,
358 H., Hansson, H. C., Vakeva, M., Koponen, I. K., Buzorius, G., and Kulmala, M.: Physical
359 characterization of aerosol particles during nucleation events, *Tellus B*, 53, 344-358, 2001.
- 360
361 Buzorius, G.: Cut-off sizes and time constants of the CPC TSI 3010 operating at 1-3 lpm flow rates,
362 *Aerosol Sci Tech*, 35, 577-585, 2001.
- 363
364 Hering, S. V. and Stolzenburg, M. R.: A method for particle size amplification by water condensation
365 in a laminar, thermally diffusive flow, *Aerosol Sci Tech*, 39, 428-436, 2005.
- 366
367 Hering, S. V., Stolzenburg, M. R., Quant, F. R., Oberreit, D. R., and Keady, P. B.: A laminar-flow, water-
368 based condensation particle counter (WCPC), *Aerosol Sci Tech*, 39, 659-672, 2005.
- 369
370 Hering, S. V., Spielman, S. R., and Lewis, G. S.: Moderated, Water-Based, Condensational Particle
371 Growth in a Laminar Flow, *Aerosol Sci Tech*, 48, 401-408, 2014.
- 372
373 Hering, S. V., Lewis, G. L., Spielman, S. R., Eiguren-Fernandez, A., Kreisberg, N. M., Kuang, C., and
374 Attoui, M.: Detection near 1-nm with a Laminar-Flow, Water-Based Condensation Particle Counter,
375 *Aerosol Sci Tech*, 2016. 2016.
- 376
377 Iida, K., Stolzenburg, M. R., and McMurry, P. H.: Effect of Working Fluid on Sub-2 nm Particle
378 Detection with a Laminar Flow Ultrafine Condensation Particle Counter, *Aerosol Sci Tech*, 43, 81-96,
379 2009.
- 380
381 Jiang, J. K., Chen, M. D., Kuang, C. A., Attoui, M., and McMurry, P. H.: Electrical Mobility
382 Spectrometer Using a Diethylene Glycol Condensation Particle Counter for Measurement of Aerosol
383 Size Distributions Down to 1 nm, *Aerosol Sci Tech*, 45, 510-521, 2011a.
- 384
385 Jiang, J. K., Zhao, J., Chen, M. D., Eisele, F. L., Scheckman, J., Williams, B. J., Kuang, C. A., and
386 McMurry, P. H.: First Measurements of Neutral Atmospheric Cluster and 1-2 nm Particle Number
387 Size Distributions During Nucleation Events, *Aerosol Sci Tech*, 45, ii-V, 2011b.
- 388
389 Kangasluoma, J., Junninen, H., Lehtipalo, K., Mikkilä, J., Vanhanen, J., Attoui, M., Sipilä, M., Worsnop,
390 D., Kulmala, M., and Petäjä, T.: Remarks on Ion Generation for CPC Detection Efficiency Studies in
391 Sub-3-nm Size Range, *Aerosol Sci Tech*, 47, 556-563, 2013.
- 392
393 Kangasluoma, J., Kuang, C., Wimmer, D., Rissanen, M. P., Lehtipalo, K., Ehn, M., Worsnop, D. R.,
394 Wang, J., Kulmala, M., and Petäjä, T.: Sub-3 nm particle size and composition dependent response of
395 a nano-CPC battery, *Atmos Meas Tech*, 7, 689-700, 2014.
- 396
397 Kangasluoma, J., Ahonen, L., Attoui, M., Vuollekoski, H., Kulmala, M., and Petäjä, T.: Sub-3 nm
398 Particle Detection with Commercial TSI 3772 and Airmodus A20 Fine Condensation Particle Counters,
399 *Aerosol Sci Tech*, 49, 674-681, 2015a.



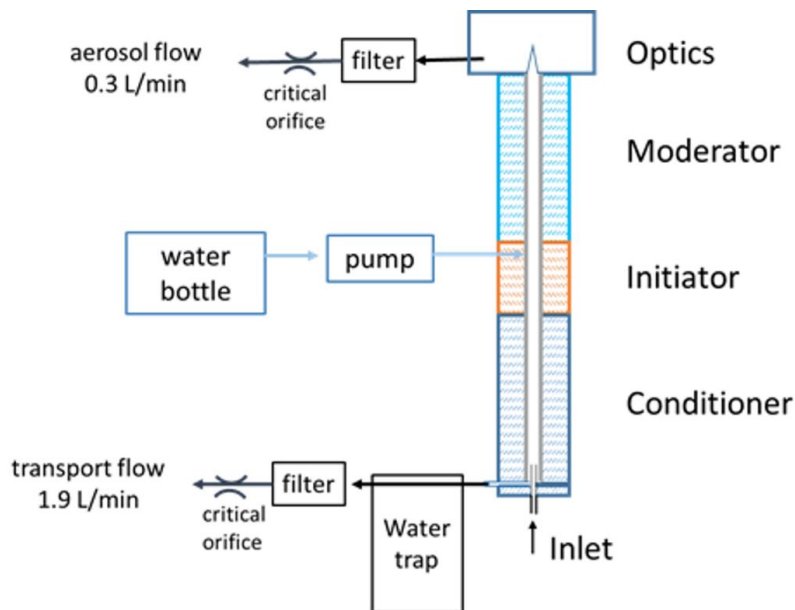
- 400
401 Kangasluoma, J., Attoui, M., Junninen, H., Lehtipalo, K., Samodurov, A., Korhonen, F., Sarnela, N.,
402 Schmidt-Ott, A., Worsnop, D., Kulmala, M., and Petäjä, T.: Sizing of neutral sub 3 nm tungsten oxide
403 clusters using Airmodus Particle Size Magnifier, *J Aerosol Sci*, 87, 53-62, 2015b.
- 404
405 Kangasluoma, J., Attoui, M., Korhonen, F., Ahonen, L., Siivola, E., and Petäjä, T.: Characterization of a
406 Herrmann type high resolution differential mobility analyzer, *Aerosol Sci Tech*, 50, 222-229, 2016a.
- 407
408 Kangasluoma, J., Samodurov, A., Attoui, M., Franchin, A., Junninen, H., Korhonen, F., Kurtén, T.,
409 Vehkamäki, H., Sipilä, M., Lehtipalo, K., Worsnop, D., Petäjä, T., and Kulmala, M.: Heterogeneous
410 nucleation onto ions and neutralized ions - insights into sign-preference, *Journal of Physical
411 Chemistry C*, 120, 7444-7450, 2016b.
- 412
413 Kuang, C., Chen, M., Zhao, J., Smith, J., McMurry, P. H., and Wang, J.: Size and time-resolved growth
414 rate measurements of 1 to 5 nm freshly formed atmospheric nuclei, *Atmos Chem Phys*, 12, 3573-
415 3589, 2012a.
- 416
417 Kuang, C., Chen, M. D., McMurry, P. H., and Wang, J.: Modification of Laminar Flow Ultrafine
418 Condensation Particle Counters for the Enhanced Detection of 1 nm Condensation Nuclei, *Aerosol
419 Sci Tech*, 46, 309-315, 2012b.
- 420
421 Kupc, A., Bischof, O., Tritscher, T., Beeston, M., Krinke, T., and Wagner, P. E.: Laboratory
422 Characterization of a New Nano-Water-Based CPC 3788 and Performance Comparison to an
423 Ultrafine Butanol-Based CPC 3776, *Aerosol Sci Tech*, 47, 183-191, 2013.
- 424
425 Lewis, G. S. and Hering, S. V.: Minimizing Concentration Effects in Water-Based, Laminar-Flow
426 Condensation Particle Counters, *Aerosol Sci Tech*, 47, 645-654, 2013.
- 427
428 Mertes, S., Schroder, F., and Wiedensohler, A.: The Particle-Detection Efficiency Curve of the Tsi-
429 3010 Cpc as a Function of the Temperature Difference between Saturator and Condenser, *Aerosol
430 Sci Tech*, 23, 257-261, 1995.
- 431
432 Okuyama, K., Kousaka, Y., and Motouchi, T.: Condensational Growth of Ultrafine Aerosol-Particles in
433 a New Particle-Size Magnifier, *Aerosol Sci Tech*, 3, 353-366, 1984.
- 434
435 Peineke, C., Attoui, M. B., and Schmidt-Ott, A.: Using a glowing wire generator for production of
436 charged, uniformly sized nanoparticles at high concentrations, *J Aerosol Sci*, 37, 1651-1661, 2006.
- 437
438 Russell, L. M., Zhang, S. H., Flagan, R. C., Seinfeld, J. H., Stolzenburg, M. R., and Caldow, R.: Radially
439 classified aerosol detector for aircraft-based submicron aerosol measurements, *J Atmos Ocean Tech*,
440 13, 598-609, 1996.
- 441
442 Seto, T., Okuyama, K., de Juan, L., and Fernández de la Mora, J.: Condensation of supersaturated
443 vapors on monovalent and divalent ions on varying size, *J Chem Phys*, 107, 1576-1585, 1997.



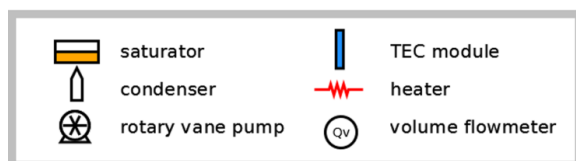
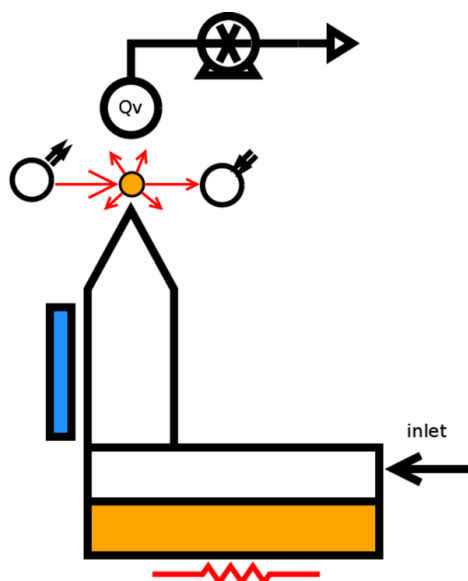
- 444
445 Sipilä, M., Lehtipalo, K., Attoui, M., Neitola, K., Petäjä, T., Aalto, P. P., O'Dowd, C. D., and Kulmala, M.:
446 Laboratory Verification of PH-CPC's Ability to Monitor Atmospheric Sub-3 nm Clusters, *Aerosol Sci*
447 *Tech*, 43, 126-135, 2009.
- 448
449 Stolzenburg, M. R. and McMurry, P. H.: An Ultrafine Aerosol Condensation Nucleus Counter, *Aerosol*
450 *Sci Tech*, 14, 48-65, 1991.
- 451
452 Ude, S. and Fernández de la Mora, J.: Molecular monodisperse mobility and mass standards from
453 electrospays of tetra-alkyl ammonium halides, *J Aerosol Sci*, 36, 1224-1237, 2005.
- 454
455 Vanhanen, J., Mikkilä, J., Lehtipalo, K., Sipilä, M., Manninen, H. E., Siivola, E., Petäjä, T., and Kulmala,
456 M.: Particle Size Magnifier for Nano-CN Detection, *Aerosol Sci Tech*, 45, 533-542, 2011.
- 457
458 Wang, Y., Kangasluoma, J., Attoui, M., Fang, J., Junninen, H., Kulmala, M., Petäjä, T., and Biswas, P.:
459 The high charge fraction of flame-generated particles in the size range below 3 nm measured by
460 enhanced particle detectors, *Combust Flame*, 176, 72-80, 2017.
- 461
462 Weber, R. J., Marti, J. J., McMurry, P. H., Eisele, F. L., Tanner, D. J., and Jefferson, A.: Measured
463 atmospheric new particle formation rates: Implications for nucleation mechanisms, *Chem Eng*
464 *Commun*, 151, 53-64, 1996.
- 465
466 Wiedensohler, A., Orsini, D., Covert, D. S., Coffmann, D., Cantrell, W., Havlicek, M., Brechtel, F. J.,
467 Russell, L. M., Weber, R. J., Gras, J., Hudson, J. G., and Litchy, M.: Intercomparison study of the size-
468 dependent counting efficiency of 26 condensation particle counters, *Aerosol Sci Tech*, 27, 224-242,
469 1997.
- 470
471 Wilson, J. C., Blackshear, E. D., and Hyun, J. H.: An Improved Continuous-Flow Condensation Nucleus
472 Counter for Use in the Stratosphere, *J Aerosol Sci*, 14, 387-391, 1983.
- 473
474 Wimmer, D., Lehtipalo, K., Franchin, A., Kangasluoma, J., Kreissl, F., Kurten, A., Kupc, A., Metzger, A.,
475 Mikkilä, J., Petäjä, T., Riccobono, F., Vanhanen, J., Kulmala, M., and Curtius, J.: Performance of
476 diethylene glycol-based particle counters in the sub-3 nm size range, *Atmos Meas Tech*, 6, 1793-
477 1804, 2013.
- 478
479 Winkler, P. M., Steiner, G., Vrtala, A., Vehkamäki, H., Noppel, M., Lehtinen, K. E. J., Reischl, G. P.,
480 Wagner, P. E., and Kulmala, M.: Heterogeneous nucleation experiments bridging the scale from
481 molecular ion clusters to nanoparticles, *Science*, 319, 1374-1377, 2008.
- 482
483



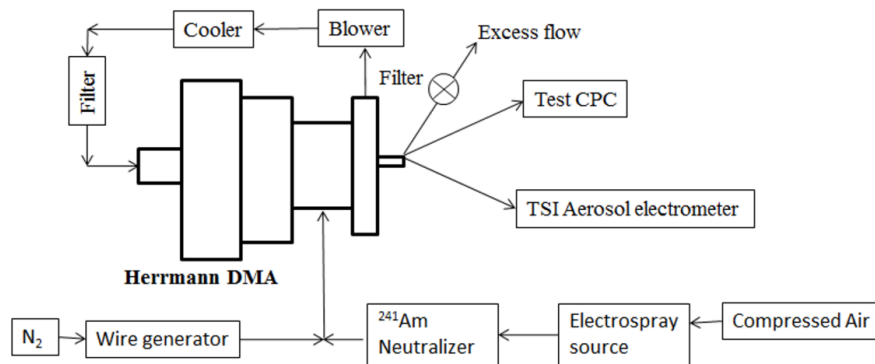
484
 485 Figure 1. TSI 3777 nano enhancer (courtesy of TSI Inc.)
 486



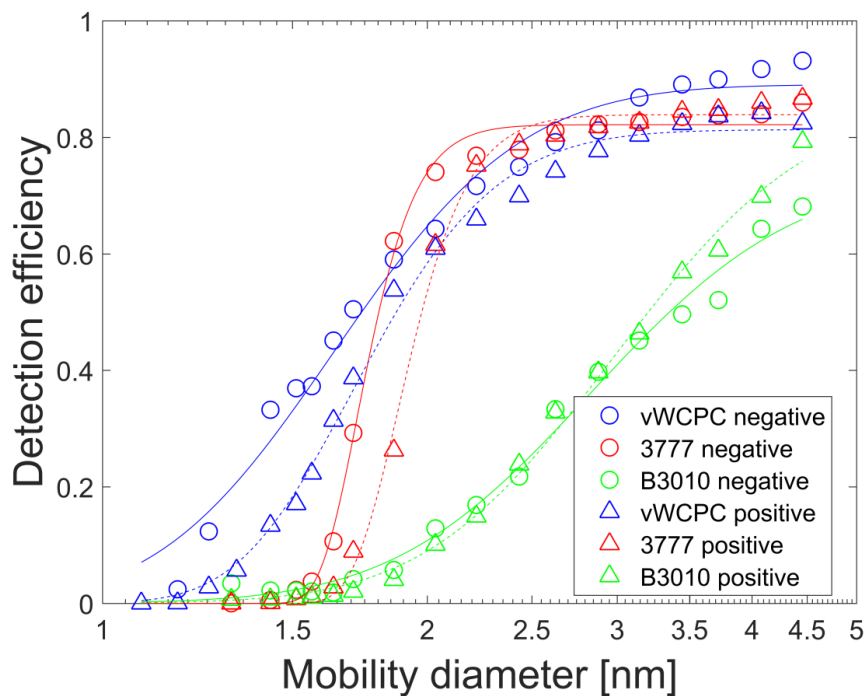
487
 488 Figure 2. ADI v-WCPC
 489



490
 491 Figure 3. B3010.
 492

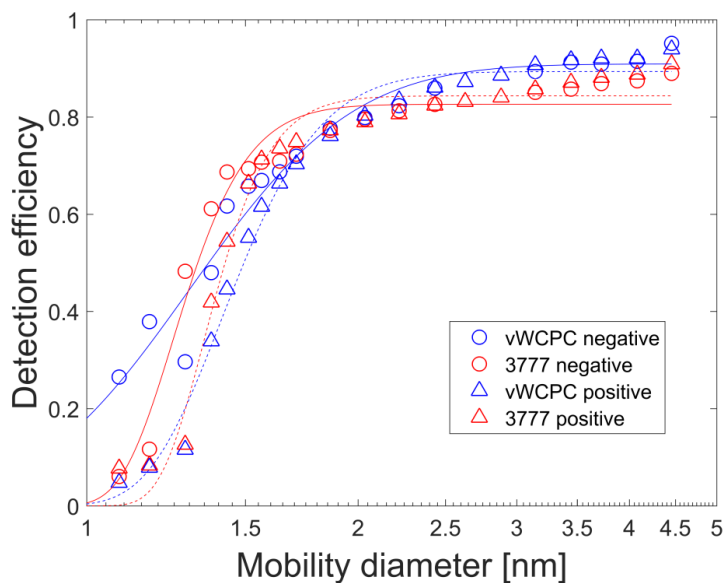


493
 494 Figure 4. Experimental setup to measure d50 for charged particles
 495
 496



497
498
499
500
501

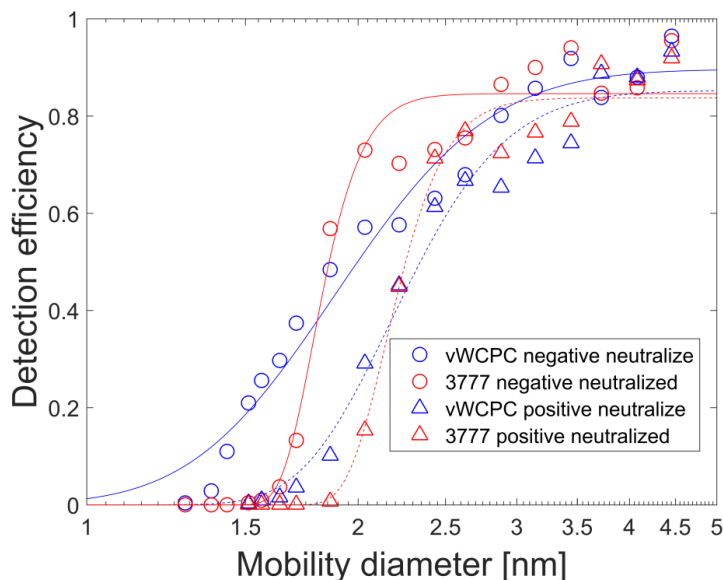
Figure 5. Detection efficiency of the CPCs as a function of size for negatively and positively charged tungsten oxide particles at low dT settings.



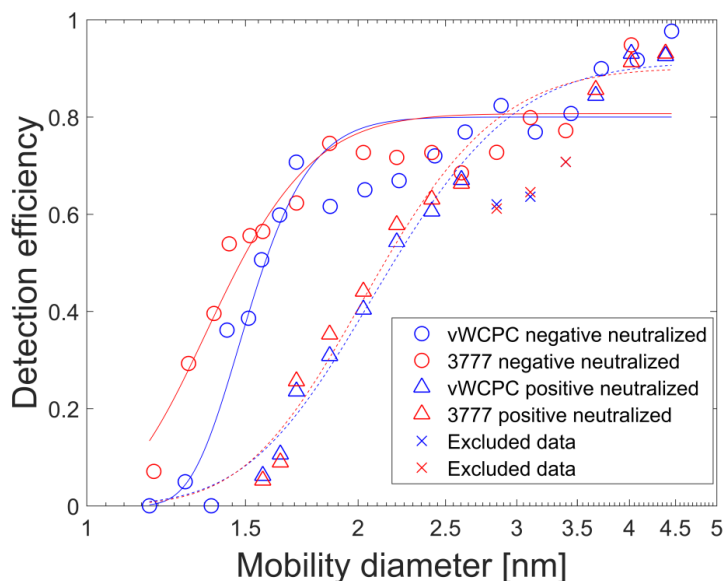
502



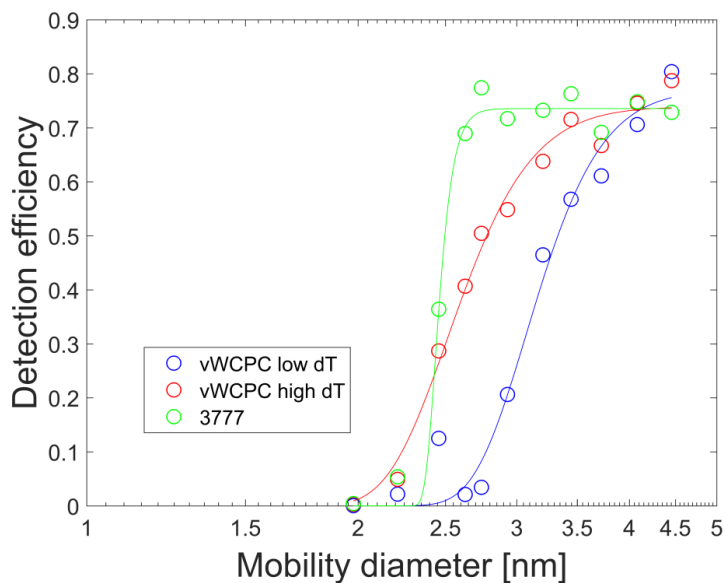
503 Figure 6. Detection efficiency of the CPCs as a function of size for positively and negatively charged
504 tungsten oxide particles at high dT settings.
505



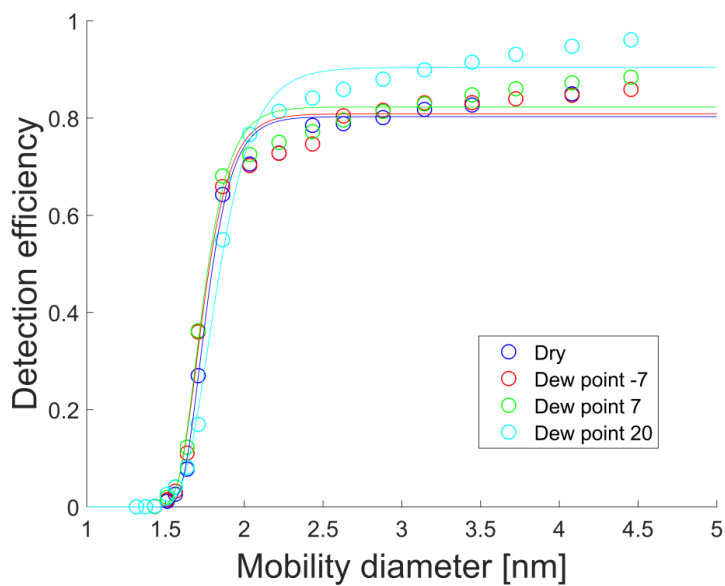
506
507 Figure 7. Detection efficiency of the CPCs as a function of size for negatively and positively charged
508 tungsten oxide particles that are neutralized at low dT settings.
509



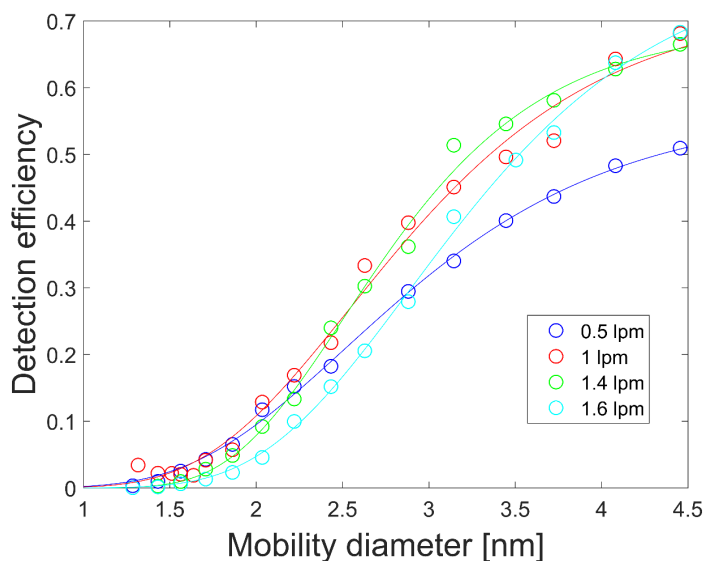
510
511 Figure 8. Detection efficiency of the CPCs as a function of size for negatively and positively charged
512 tungsten oxide particles that are neutralized at high dT settings.
513



514
515 Figure 9. Detection efficiency of the CPCs as a function of size for positively charged TDDABr particles
516 at low and high dT settings for v-WCPC and at low dT settings for the 3777.
517

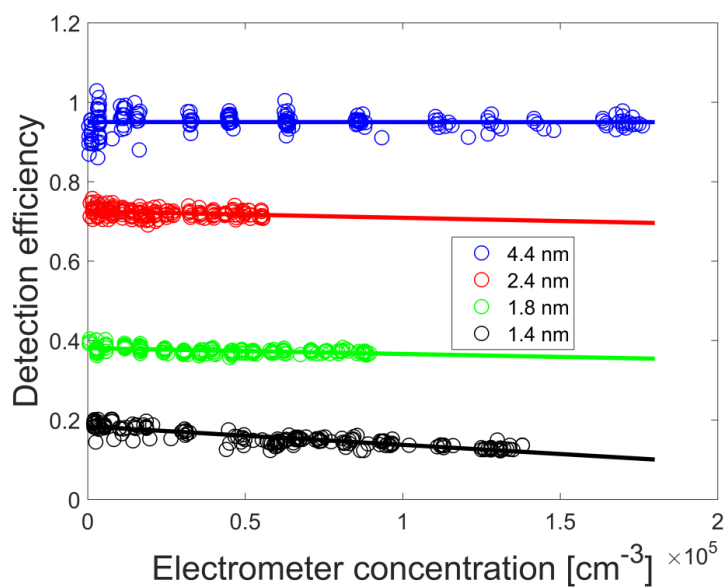


518
519 Figure 10. Detection efficiency of the 3777 as a function of the diameter and sample flow relative
520 humidity.
521



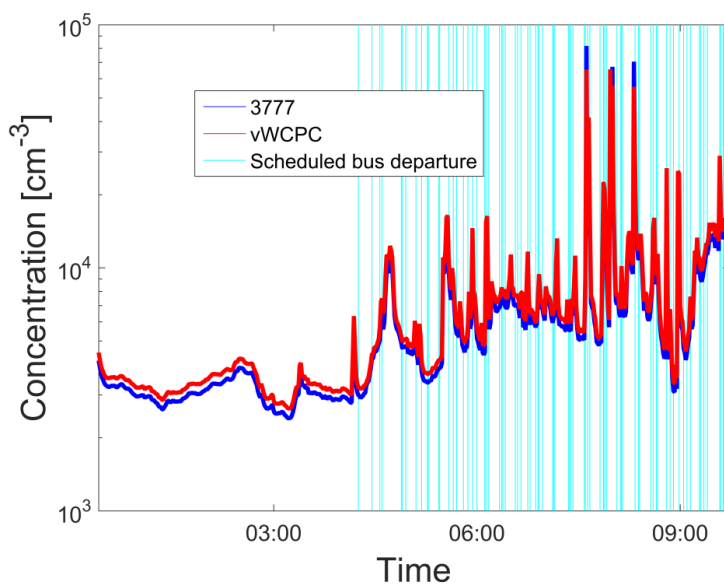
522
 523
 524

Figure 11. Detection efficiency of the B3010 as a function of the inlet flow rate.

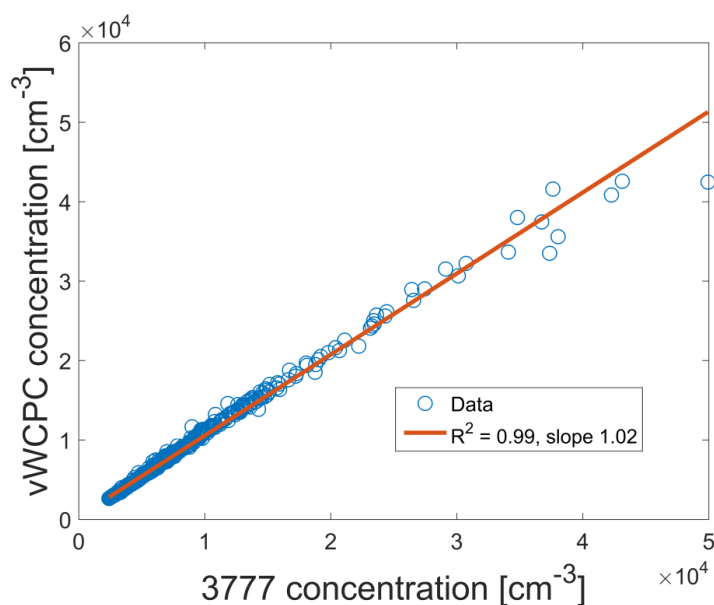


525
 526
 527

Figure 12. Ratio of the v-WCPC to the electrometer as function of the particle concentration.



528
529 Figure 13. Concentration measured by the 3777 and v-WCPC from urban atmospheric air.
530



531
532 Figure 14. Correlation of the concentrations below 50 000 cm⁻³ measured by the CPCs for the same
533 data as in Figure 13.
534
535
536
537
538



539

540 Table 1. Instrument operation conditions

| Instrument | Qinlet [lpm] | Qaerosol [lpm] | Settings | Ts [oC] | Tc [oC] | Tm [oC] | To [oC] |
|------------|-----------------|-------------------|----------|------------|------------|------------|------------|
| B3010 | 1 | 1 | Low dT | 55 | 10 | | 56 |
| vWCPC | 2.2 | 0.3 | Low dT | 8 | 90 | 22 | 40 |
| vWCPC | 2.2 | 0.3 | High dT | 1 | 95 | 22 | 40 |
| 3777 | 2.5 | 0.15 | Low dT | 62 | 12 | | |
| 3777 | 2.5 | 0.15 | High dT | 70 | 7 | | |

541

542

543 Table 2. Indicated Cutpoints

| Conditions | Aerosol | Charging state | ADI v-WCPC | TSI-3777 | B3010 |
|------------|---------|----------------|------------|----------|-------|
| High dT | WOx | negative | 1.4 | 1.3 | NA |
| High dT | WOx | positive | 1.5 | 1.4 | NA |
| High dT | WOx | neutral from - | 1.6 | 1.5 | NA |
| High dT | WOx | neutral from + | 2.2 | 2.1 | NA |
| Low dT | WOx | negative | 1.7 | 1.8 | 3.4 |
| Low dT | WOx | positive | 1.9 | 2 | 3.2 |
| Low dT | WOx | neutral from - | 2 | 1.9 | NA |
| Low dT | WOx | neutral from + | 2.4 | 2.3 | NA |
| High dT | TDDAB | positive | 2.8 | NA | NA |
| Low dT | TDDAB | positive | 3.3 | 2.5 | NA |

544

545